ELSEVIER

Journal of Nuclear Materials 303 (2002) 156–168

journal of nuclear materials

www.elsevier.com/locate/jnucmat

# Synthesis and characterization of nanocrystalline thoria obtained from thermally decomposed thorium carbonate

S. Dash [a,*], A. Singh [a], P.K. Ajikumar [a], H. Subramanian [b], M. Rajalakshmi [a], A.K. Tyagi [a], A.K. Arora [a], S.V. Narasimhan [b], Baldev Raj [a]

[a] *Metallurgy and Materials Group, Indira Gandhi Centre for Atomic Research, Kalpakkam 603 102, India*
[b] *Water and Steam Chemistry Laboratory, BARC Facilities, Kalpakkam 603 102, India*

Received 11 December 2001; accepted 25 February 2002

---

## Abstract

Nanocrystalline thoria was synthesized by temperature programmed decomposition of $Th(CO_3)_2$ in an evolved gas analysis mass spectrometer set-up. The structural and stoichiometric changes encountered in the decomposition pathway were studied by off-line thermogravimetry (TGA), X-ray diffraction and X-ray photoelectron spectroscopy (XPS). Accurate conversion temperature for transformation of $Th(CO_3)_2 \rightarrow ThO_2$ was arrived from the XPS measurements. Fourier transform infrared (FT-IR) measurements were used to compare vibrational activities of nano and bulk polycrystalline thoria. Raman spectroscopic studies indicated optical phonon confinement effects in nanocrystalline thoria. High resolution transmission electron microscopic examination on starting material, intermediates and nanocrystalline final product were carried out for studying the microstructure in the nanometer scale. © 2002 Elsevier Science B.V. All rights reserved.

*PACS:* 07.75.+h; 33.60.Fy; 61.46.+w; 81.70.Pg; 82.30.Lp

---

## 1. Introduction

$Th(CO_3)_2$ occurs as an intermediate material in the calcination steps of a good number of thoria precursors [1]. These are oxalates, ammonium thorium carbonate and formates. The understanding of thermal and structural behavior of $Th(CO_3)_2$ would definitely aid choice of appropriate temperature window required for synthesis of nanocrystalline thoria. There is also a need to study stoichiometric evolution of nanocrystalline thoria with minimum carry over of impurity phases during synthesis. Due to superior sintering behavior, nanocrystalline thoria is excitingly promising for a thorium based fuel cycle envisaged in the fabrication of fast breeder reactors (FBRs) and advanced heavy water reactors (AHWR) fuel material [2,3]. In the light of the above, the present investigation focuses at characterization of nanocrystalline thoria obtained by temperature programmed transformation of $Th(CO_3)_2$. This was carried out in an evolved gas analysis-mass spectrometry (EGA-MS) system. Stoichiometric investigations were also carried out using a non-isothermal TGA apparatus. Phase evolution of nanocrystalline thoria was studied by powder X-ray diffraction (XRD). High resolution transmission electron microscopy (HRTEM) was used to study morphology of thoria and its precursors. Fourier transform infrared (FT-IR) spectroscopy was used to study extent of functional group loss and additional vibrational features associated with nanocrystalline thoria. Raman spectroscopic measurements were used to study changes in the optical phonon line shape associated with nanocrystalline thoria. X-ray photoelectron spectroscopy (XPS) measurements were used to study alteration in the chemical environment of the thorium atoms and completion of thorium carbonate to thoria conversion. The latter information was derived

---

[*] Corresponding author. Tel./fax: +91-4114 480 081.
*E-mail address:* dash@igcar.ernet.in (S. Dash).

0022-3115/02/$ - see front matter © 2002 Elsevier Science B.V. All rights reserved.
PII: S0022-3115(02)00816-4

from O/M photoelectric peak intensity ratio measurements.

## 2. Experimental

GR grade anhydrous $Th(CO_3)_2$ powder sample procured from BDH chemicals, UK, was used in all our investigations. The scanning electron micrographs revealed polyhedral particles having dimensions ranging between 1 and 5 μm. A typical SEM micrograph is shown in the Fig. 1. The trace metallic constituents in this compound were determined using an ELAN 250, SCIEX, Canada, inductively coupled plasma mass spectrometer (ICP-MS) [4]. The samples were dissolved in spectroscopically pure reagents and sprayed to ICP by use of a peristaltic pump and Meinhard nebulizer [5]. The data was acquired in the rapid scan mode. The instrument was calibrated using synthetic spectroscopically pure NBS traceable standards. Concentration of metallic impurities was found to be in μg/g level. Many of the impurities were detected but could not be quantified as their levels were found to be below blank (solvent reagent) values. These are presented in Table 1.

Hundred mg of the sample was used for each run. The EGA-MS runs were performed at a heating rate of 5 K/min in the temperature span 300–1000 K. Also one run was conducted up to 1200 K.

A polycrystalline thoria sample for purpose of generating reference data was prepared in a furnace by heating thorium carbonate up to 1700 K for 4 h. The experimental details of the EGA-MS facility used to conduct temperature programmed decomposition (TPD) runs has been described elsewhere [6–8]. However, for the sake of completeness a brief description will be furnished here. The facility essentially consists of a high temperature (∼1400 K), high vacuum programmable resistance furnace connected to an ultrahigh vacuum (UHV, $10^{-10}$ m) chamber by a variable conductance molecular leak valve. The high vacuum chamber is evacuated to a base pressure of $10^{-7}$ mbar by a turbo molecular pumping (TMP) system. The UHV chamber housing quadrupole mass spectrometer (QMS) and other metrological hardware like spinning rotor viscosity gauge (SRG) is pumped by an ion sublimation pump (ISP). The ISP interior as well as the UHV chamber are roughed by a separate TMP. The UHV chamber is also

Table 1
Concentration of trace metallic impurities in $Th(CO3)_2$ as analyzed by ICP-MS

| Elements | Concentration (μg/g) |
|---|---|
| Al | <15 |
| Ba | 80 |
| Co | <15 |
| Cu | <15 |
| Cr | <15 |
| Fe | <20 |
| V | <15 |
| Mn | <15 |
| Mo | <15 |
| Ni | <15 |
| Pb | <15 |
| Sr | <15 |
| Ti | <15 |
| Zn | <15 |

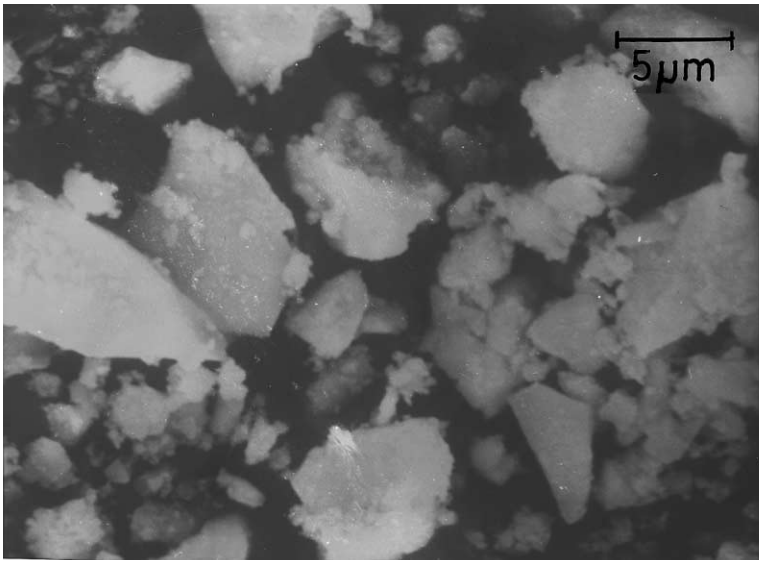

Fig. 1. Scanning electron micrograph of $Th(CO_3)_2$ raw powder.

equipped with gas inlets to enable system calibration. The QMS is operated in real time multiple ion detection (MID-MS) mode. A data logger (HP Agilent 34970 A) acquires the MID signals as well as the linearly rising sample temperature. A plot of MID signal against absolute temperature yields TPD spectra. Calibrated K-type thermocouples (two numbers) are used for acquisition of sample temperature.

The TGA runs of the $Th(CO_3)_2$ were conducted in a SETRAM, France manufactured SETSYS$^{TM}$ 16/18 thermal analysis system with 5 K/min heating rate. An ultrahigh pure (UHP 99.99%) helium carrier gas flow at a rate of 40 ml/min was maintained during the run. To enable suitable comparison, the EGA-MS and TGA runs were conducted at similar heating rates in the temperature span 300–1000 K. Prior to acquisition of these thermograms, the TGA/DTA machine was temperature-calibrated by recording melting endotherms of UHP metals Sn, Zn and Al [9]. The thermograms were correlated for buoyancy and background. However, minor discrepancy between TGA and EGA-MS inflexion temperatures were noticed due to different sample environments. For the purpose of condensed phase characterization by FT-IR, Raman spectroscopy, XRD, HRTEM and XPS, the samples were heated till completion of various gas release stages. The temperature programme was interrupted after each gas release stage. This was done by visually observing the EGA-MS spectra falling to the background. Samples were also prepared at 1000 and 1200 K by heating the $Th(CO_3)_2$ beyond decomposition regime. A bulk polycrystalline compound of thoria was synthesized by heating the $Th(CO_3)_2$ to 1700 K.The initial compound, residues and the final bulk polycrystalline compounds are designated as following:

| | | |
|---|---|---|
| A | Raw sample | 300 K |
| B | Completion of stage I $CO_2$ release | 585 K |
| C | Sample after stage II $CO_2$ release | 800 K |
| D | Sample heated beyond decomposition regime (I) | 1000 K |
| E | Sample heated beyond decomposition regime (II) | 1200 K |
| F | Bulk polycrystalline thoria | 1700 K |

The FT-IR spectra of these residues were acquired with the help of a M/S BOMEM, Canada make DA8 FT spectrometer. The mid-IR spectrum was acquired with KBr optics in the 500–4500 cm$^{-1}$ wave number span. The far IR spectra were obtained with CsI optics in the span 100–700 cm$^{-1}$. These spectra were acquired in the transmission mode.

Raman spectra of nanocrystalline and well characterized polycrystalline powders of $ThO_2$ were recorded in the back scattering geometry and room temperature using a set-up described elsewhere [10]. About 100 mW of power at 482.5 nm line from an argon ion laser (Coherent, I-90) was used for exciting the Raman spectra. The scattered light from the sample was analysed using a double monochromator (Spex, 14018) and detected using a cooled photomultiplier tube operated in the photon counting mode. Scanning of the spectra and data acquisition were done using a microprocessor based data acquisition-cum-control system.

A Siemens D-500 powder X-ray diffractometer working in Bragg–Brentano diffraction geometry and equipped with a sample spinner was used to acquire diffractograms. Powdered samples were mounted in the form of a thin layer on a zero background Si(9 1 1) substrate using Cu($K_\alpha$) as incident radiation. The scattered intensities were recorded in the $2\theta$ span of 10–70°. Prior to spectral acquisition the instrument was properly aligned and checked for its figure of merit by conducting a run on α-quartz. JCPDS-ICDD sticks were used to carry out spectral indexing. The particle size of the nanocrystalline products were determined by using Scherrer formula given as

$$t = 0.9\lambda/\beta\cos\theta_B, \tag{1}$$

where $t$ indicates particle size in nanometers and $\lambda$ the incident X-ray wavelength [11]. In the present case, $\lambda$ was assumed to be 0.154183 nm, which is the weighted average of Cu-$K_{\alpha1}$ and Cu-$K_{\alpha2}$ lines. $\beta$ is the radian measure of the full width at half maximum of the peak intensity. $\theta_B$ refers to the Bragg angle subtended at maximum intensity. In our particle size analysis, machine contribution to the broadening was subtracted from the observed FWHM.

For observation in HRTEM, the powder specimens obtained from the EGA-MS machine were dispersed in analytical grade methyl alcohol and agitated in an ultrasonic cleaner for few minutes. A drop of this supernatant liquid was put onto a 200 mesh (3 mm diameter) copper grid coated with a holey carbon film and transferred to TEM load lock. The TEM studies were carried out on a JEOL JEM 2000 EX II electron microscope operating at 200 kV. With HRTEM, the high resolution lattice imaging as well as selected area electron diffraction (SAED) patterns were acquired.

XPS measurements were carried out with a VG ESCALAB MK 200 X ESCA machine using Al-$K_\alpha$ X-ray source (1486.60 eV) and hemispherical mirror analyzer that was operated at a band pass energy of 20 eV giving an analyzer resolution of 0.4 eV. Here again, a thin layer of powder sample was strapped to a 0.5 mm UHP indium metal foil. This was quickly loaded into the analysis chamber of the ESCA machine to avoid moisture ingress. The binding energy was calibrated with Au($4f_{7/2}$) photoelectron peak at 84.0 with a 1.6 eV FWHM for a specimen of Au film on Si substrate. To measure chemical shifts, the metallic thorium value

($Th^{0+}$ $4f_{7/2}$), taken from the literature, was used as a reference.

## 3. Kinetic analysis

Single particle decomposition behavior of the anhydrous $Th(CO_3)_2$ was studied by using non-isothermal kinetics [12]. Fractional extent of gas evolution/fractional extent of weight loss was used to obtain analytical expressions in terms of $f(\alpha)$. The integral model function $g(\alpha)$ was obtained as follows:

$$d(\alpha)/dt = k(T)f(\alpha), \tag{2}$$

where $k(T)$ is temperature dependent rate constant expressible as

$$k(T) = Z\exp(-E/RT), \tag{3}$$

where $Z$ is pre-exponential factor and $E$ is the activation energy, $R$ is universal gas constant and $T$ denotes the absolute temperatures. At any given instant of time $T$ can be written as

$$T = T_0 + \beta t, \tag{4}$$

where $\beta = dT/dt$ is the heating rate. Suitable substitution leads to the analytical expression

$$\int_0^{\alpha} \frac{d\alpha}{f(\alpha)} = (Z/\beta)\int_0^{T} \exp(-E/RT)\,dT. \tag{5}$$

With necessary expansions and solutions, the equation simplifies to

$$\ln[g(\alpha)/T^2] = \ln(ZR/\beta E) - E/RT.$$

A plot of $\ln[g(\alpha)/T^2] \sim 1/T$ yields a straight line whose intercept and slope gives $\ln(ZR/\beta E)$ and $E/R$, respectively [12].

Suitable correlation with experimental data is used to obtain the rate governing expression. A list of $g(\alpha)$ expressions used for the above purpose is given in Table 2 [13].

## 4. Results and discussion

### 4.1. TGA/DTA and EGA-MS studies

$Th(CO_3)_2$ depicts 25% weight loss in the temperature span 300–900 K. The weight loss commences just above the room temperature without any induction period. Simultaneous DTA run indicated completely endothermic nature of the process. Fig. 2 gives a TPD plot of $Th(CO_3)_2$. The plot shows TGA spectra superimposed with DTA and EGA-MS spectra. The TGA and EGA-MS spectra appeared to be multistep in nature. Mathematical deconvolution of TGA spectra is shown in the Fig. 3. Two weight loss stages, one spanning 300–500 K and the other one covering 500–900 K are clearly observed.

The loss of 25% weight in two stages can be accounted by loss of two molecules of $CO_2$ from $Th(CO_3)_2$ lattice. The loss of each molecule accounts for 12.5% of the total weight. This is further corroborated by the EGA-MS results. The deconvoluted EGA-MS spectra are shown in Fig. 4. The EGA spectral deconvolution also revealed occurrence of two distinct gas evolution stages spanning 300–900 K. Based on these observations, it can be stated that the decomposition of

Table 2
Integral form of non-isothermal kinetic rate expressions

| Reaction mechanism | Symbol | $g(\alpha) = \int_0^{\infty} d\alpha/f(\alpha)$ |
|---|---|---|
| *Nucleation and growth models* | | |
| Random nucleation approach | | |
| (i) Mampel unimolecular law | A1 | $-\ln(1-\alpha)$ |
| (ii) Avrami–Erofeev nuclei growth: | A(n) | $[-\ln(1-\alpha)]^{1/n}$ |
| (iii) Branching nuclei: (Prout–Tompkins) | B1 | $\ln[\alpha/(1-\alpha)]$ |
| *Decelerating rate equations* | | |
| *(a) Based on diffusion mechanism* | | |
| (i) one-dimensional diffusion | D1 | $\alpha^2/2$ |
| (ii) two-dimensional diffusion | D2 | $(1-\alpha)[\ln(1-\alpha)]+\alpha$ |
| (iii) three-dimensional diffusion (Jander) | D3 | $3/2[1-(1-\alpha)^{1/3}]^2$ |
| (iv) three-dimensional diffusion (Ginstling–Brounshtein) | D4 | $3/2[1-2\alpha/3-(1-\alpha)^{2/3}]$ |
| *(b) Based on phase boundary movement* | | |
| (i) one-dimensional (zero order) | R1 | $\alpha$ |
| (ii) two-dimensional (cylindrical symmetry) | R2 | $2[1-(1-\alpha)^{1/2}]$ |
| (iii) three-dimensional (spherical symmetry) | R3 | $3[1-(1-)^{1/3}]$ |

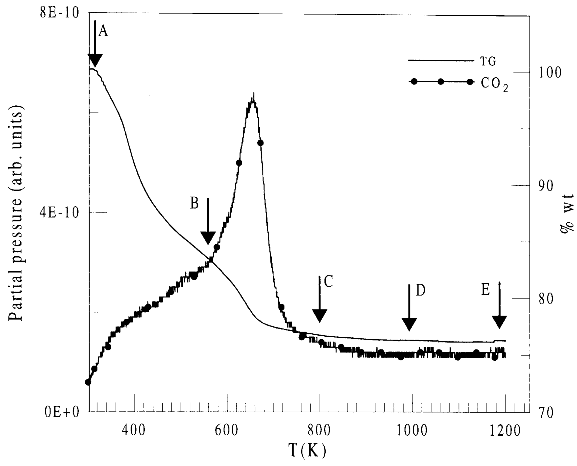

Fig. 2. TPD spectra of $Th(CO_3)_2$ showing TGA and EGA-MS plots.

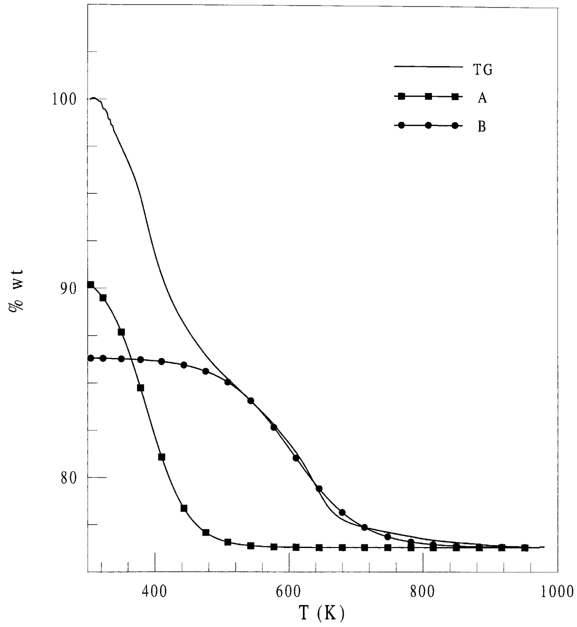

Fig. 3. Deconvoluted TGA spectra of $Th(CO_3)_2$ showing two distinct weight loss stages.

$Th(CO_3)_2$ proceeds in two steps. In first step, it converts to $ThOCO_3$ and then to $ThO_2$.

The kinetic analysis was conducted on the fraction release plots (Fig. 5). The decomposition mechanism involved in both the stages were found to be controlled by Mampel unimolecular law governed by random nucleation approach. This is expected as freshly exposed reactant surface continue to appear with desorption of $CO_2$ gas from the lattice. Also, the high specific surface associated with the nanocrystalline nature of the reacting species makes random nucleation mechanism dominant rate governing expression. The activation energy, pre-exponential factor and correlation co-efficients are given in Table 3. There is a difference in values of Arrhenius parameters obtained from TGA and EGA-MS data. The reason can be attributed to differing decomposition environments [14].

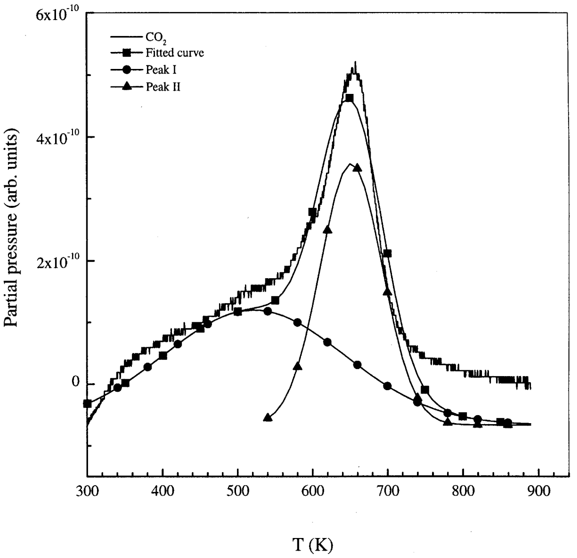

Fig. 4. Deconvoluted EGA-MS spectra of $Th(CO_3)_2$ showing two distinct $CO_2$ release stages.

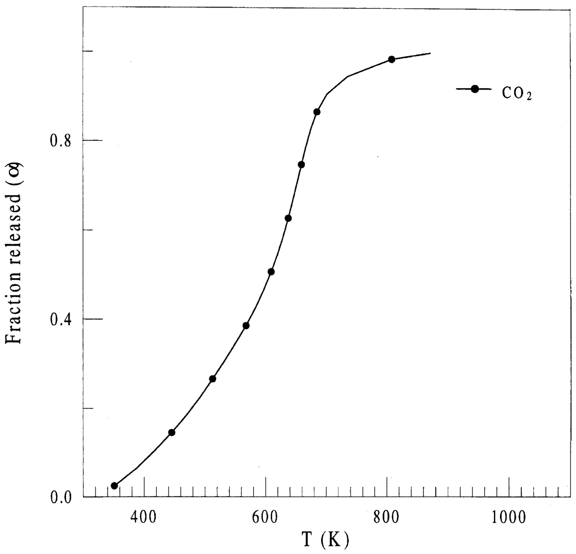

Fig. 5. Fractional release plot ($\alpha_{(T)} \sim T$) obtained from EGA-MS spectra.

Table 3
Activation energy, pre-exponential factor and correlation co-efficient for various gas release stages

| Experimental method | Conversion steps | Activation energy ($E$) (kJ/mol) | Pre-exponential factor ($Z$) ($s^{-1}$) | Correlation coefficient |
|---|---|---|---|---|
| EGA-MS | $Th(CO_3)_2 \rightarrow ThOCO_3$ | 23.896 | 6.9373 | 0.997 |
| | $ThOCO_3 \rightarrow ThO_2$ | 109.841 | $7.3 \times 10^7$ | 0.996 |
| TGA | $Th(CO_3)_2 \rightarrow ThOCO_3$ | 28.309 | 555 | 0.991 |
| | $ThOCO_3 \rightarrow ThO_2$ | 24.58 | 4.05 | 0.999 |

## 5. Infrared spectroscopic studies

FT-IR spectroscopic measurements on various intermediates were conducted in the mid-IR as well as in the far IR regimes. The mid-IR data are plotted in Fig. 6. In these spectra, vibrations associated with carbonate ligand are clearly depicted. In raw $Th(CO_3)_2$ sample, a broad absorption band having a doublet structure was observed in the wave number regime 1200–1800 $cm^{-1}$. Though no prior information exists on infrared spectroscopic study of thorium carbonate, spectral comparison with other carbonates leads to this inference [15]. The area intensity of the band diminishes with the advancement of temperature programme. At 1000 K, these absorption features completely disappear. This signifies complete conversion of thorium carbonate to thoria as inferred from the loss of characteristic group frequency observed in the 1000–1900 wave numbers. An asymmetric dip in the transmission also occurs in the 1900–3700 wave number regime. This asymmetric valley gradually disappears with the increase in temperature. At 1000 K, conversion to nanocrystalline thoria occurs. This particular band reappears in microcrystalline thoria probably due to blurring of vibrational levels.

The far IR spectra (Fig. 7) which normally yields information on metal–ligand coordination and lattice modes indicated asymmetric but well defined vibrational

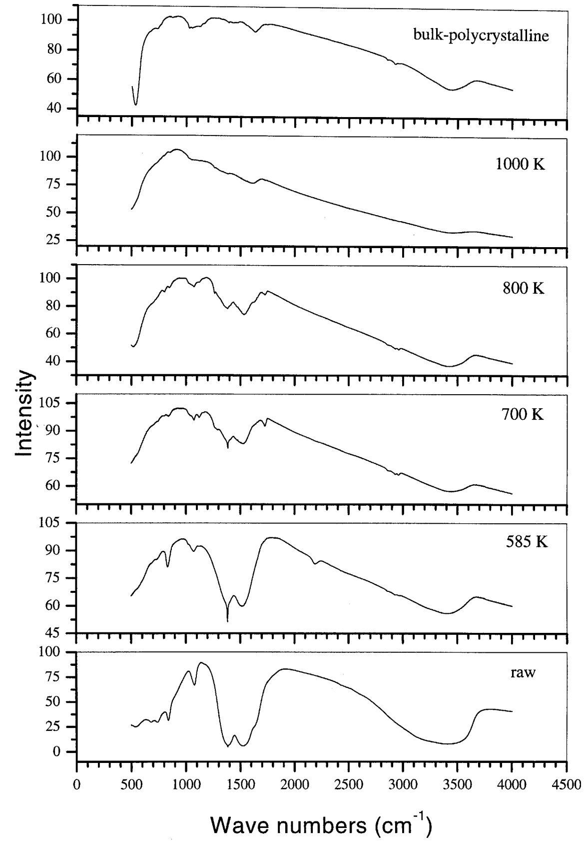

Fig. 6. Mid FT-IR spectra of $Th(CO_3)_2$ and various residues.

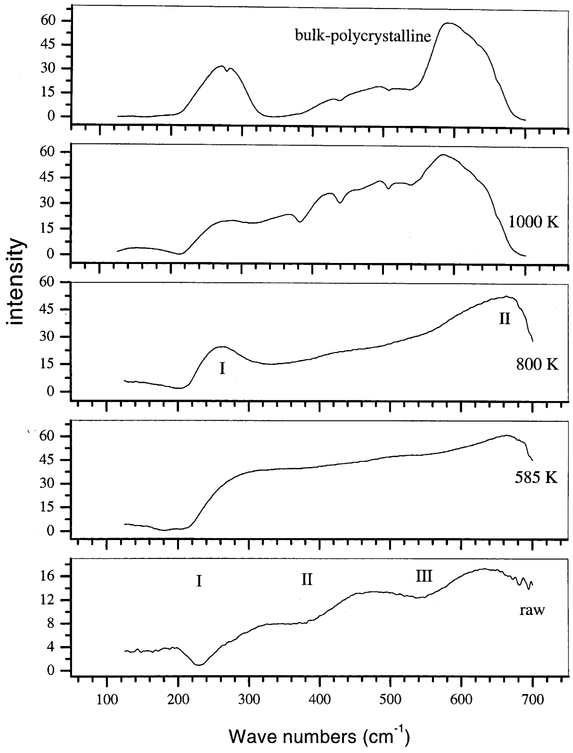

Fig. 7. Far FTIR spectra of $Th(CO_3)_2$ and various residues.

bands marked as I, II, III. In stage B compound these levels disappear and an improvement in transmission occurs. At 800 K well defined transmission bands appear (marked I and II). These transmission bands are symmetrically poised. The vibrational levels in microcrystalline thoria are somewhat blurred. The reason behind blurring can be attributed to the loss of discretization of vibrational levels. Similarly, reduced transmittance in nanocrystalline thoria arises from enhanced scattering of light by the defects and grain boundaries that are abundant in nanocrystalline materials [16].

## 6. Raman spectroscopy

Fig. 8 shows Raman spectra of bulk (well crystallized polycrystalline powder) and nanocystalline thoria samples. Thoria has fluorite structure ($Fm\bar{3}m$ space group) and exhibits only one Raman active optical phonon mode of $F_{2g}$ symmetry. It may be noted that the Raman spectrum of the nanocrystalline thoria sample with an average particle size of ~6 nm (estimated from the X-ray analysis) exhibits a broad asymmetric peak around 461 $cm^{-1}$. On the other hand, the bulk polycrystalline thoria sample shows a narrow Raman peak at 464 $cm^{-1}$. The frequency of the optical phonon was found to shift to lower values as the particle size is reduced and the line width was found to increase further. These changes in the Raman spectra of nanoparticles as compared to that of the bulk polycrystalline powder arise due to confinement of optical phonon within the particles [17].

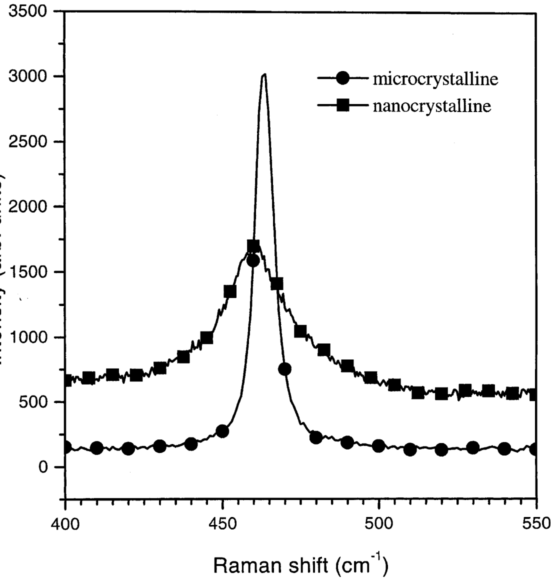

Fig. 8. Raman spectra of bulk polycrystalline and nanocrystalline thoria.

Absence of periodicity beyond the particle dimension leads to the relaxation of the $k = 0$ selection rule of Raman scattering, where $k$ is the scattering vector. This causes Raman spectrum to have contributions also from the phonons away from the Brillouin-zone center. The broadening and the shift of the Raman line has been found to depend on the shape of the phonon dispersion curve [18].

## 7. XRD studies

XRD studies showed that $Th(CO_3)_2$ appear to possess a cubic structure with high degree of structural disorder and reduced crystallinity as inferred from the broad FWHMs. Such structural disorders are invariably found in alkali and alkaline earth carbonates [19]. The powder diffractograms are shown in Fig. 9. Crystal structure of other carbonates like $Na_2CO_3$, $UO_2CO_3$ and $Bi_2O_2CO_3$ as well as the well studied structure of $CaCO_3$ generally consist of layered structural frame-

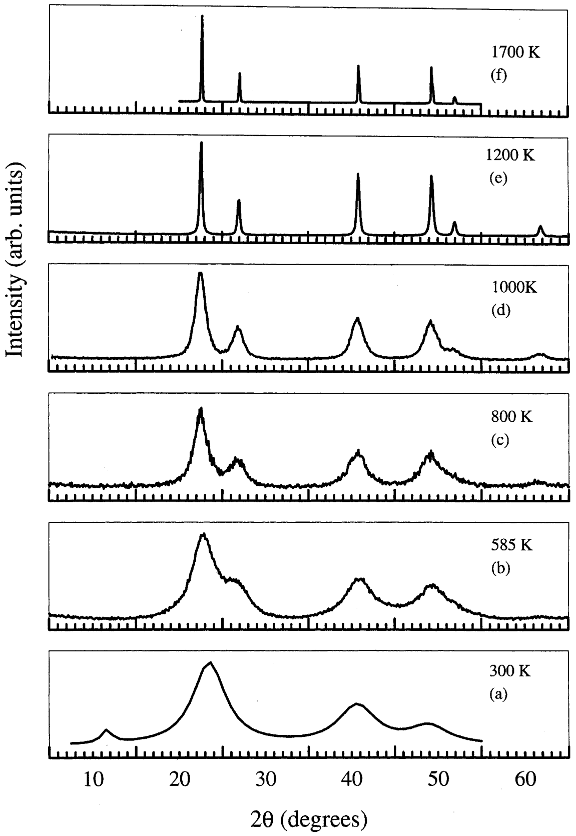

Fig. 9. Powder X-ray diffractogram of (a) $Th(CO_3)_2$, (b) $ThOCO_3$, (c) nanocrystalline thoria at 800 K, (d) nanocrystalline thoria at 1000 K, (e) nanocrystalline thoria at 1200 K and (f) bulk polycrystalline thoria at 1700 K.

work where metal atoms share oxygen from nearly planar carbonate ligands to form octahedral coordination sphere [20–23]. This local coordination framework is very often retained notwithstanding the thermally induced transformation leading to formation of corresponding metal oxides. It is also reported that such crystalline reconstruction merely involves liberation of $CO_2$ gas from cleaved carbonate ligand [22]. An electron diffraction study conducted on calcite → calcia transformation points to adjustment of calcite cleavage planes to cubic dimensions with $CO_2$ gas loss [24]. In addition to this, various studies also reveal presence of considerable amount of orientational disorder associated with $CO_3^{2-}$ group. This is inferred from the oxygen atom location. The diffraction patterns of thorium carbonates synthesized by various procedures and the presently used material (commercially supplied) match exactly. The diffraction pattern of other intermediates derived from $Th(CO_3)_2$ have been acquired after recorded loss of stoichiometry. From the broad peak of initial sample coupled with SEM observations pointing to larger particle size, it is prudent to assume that the peak broadening in $Th(CO_3)_2$ can be ascribed to stem partly from nanocrystallinity associated with grains of $Th(CO_3)_2$ particles and partly from orientational disorder normally associated with carbonate group present in the material. Close proximity of peak positions in successive diffractograms indicate that the material has undergone progressive stoichiometric simplification with the loss of facile $CO_2$ entity without significantly affecting the Th–O cubic framework.

The carbonate oxyanion as revealed from TGA and EGA studies clearly undergoes a two stage decomposition. The compound initially transforms to $ThOCO_3$ intermediate. The oxycarbonate intermediate also depicts similar diffraction characteristics indicating persistence of weak crystallinity. This compound is formed at 585 K. The increase of temperature programme to 800 K resulted in loss of last $CO_2$ functional group from the oxycarbonate ligand and transformed the material to nanocrystalline thoria with a cubic $Fm\bar{3}m$ symmetry [25]. Further increase in temperature programme beyond decomposition regime caused contraction in FWHM of diffraction peaks indicating grain growth driven increase in the particle size at 1000 and 1200 K. The nanocrystalline character is still revealed. The XRD examination was also conducted for polycrystalline thoria (Fig. 9(e)) obtained by heating $Th(CO_3)_2$ to 1700 K in the TGA furnace. This was used as our reference diffractogram.

## 8. XPS studies

In $Th(CO_3)_2$, Th has got +4 oxidation state. The electronic configuration of Th is [Rn] $4f^0 6d^2 7s^2$. The 5f shell is unoccupied. The variable valence resulting from f–d–s hybridization is not observed in the thorium compounds. In all our XPS investigations on $Th(CO_3)_2$ and its temperature program derived intermediates the thorium oxidation state remained unaltered. However, the temperature program did alter the chemical coordination surrounding the thorium cation. The bonding valence band involving Th 6d and 7s levels and 2s–2p levels of the oxygen ligand always underwent subtle but observable reorganization. This was observed in the minor fluctuation of chemical shift of the thorium photoelectric peaks. Also a notable effect of such chemical reorganization was reflected in the variation of satellite peak area. As the temperature program involved desorption of oxygen bearing groups, alteration in oxygen photoelectric peak area was also observed. The temperature program as reported earlier also leads to persistence of carry over phases at various steps. Ion

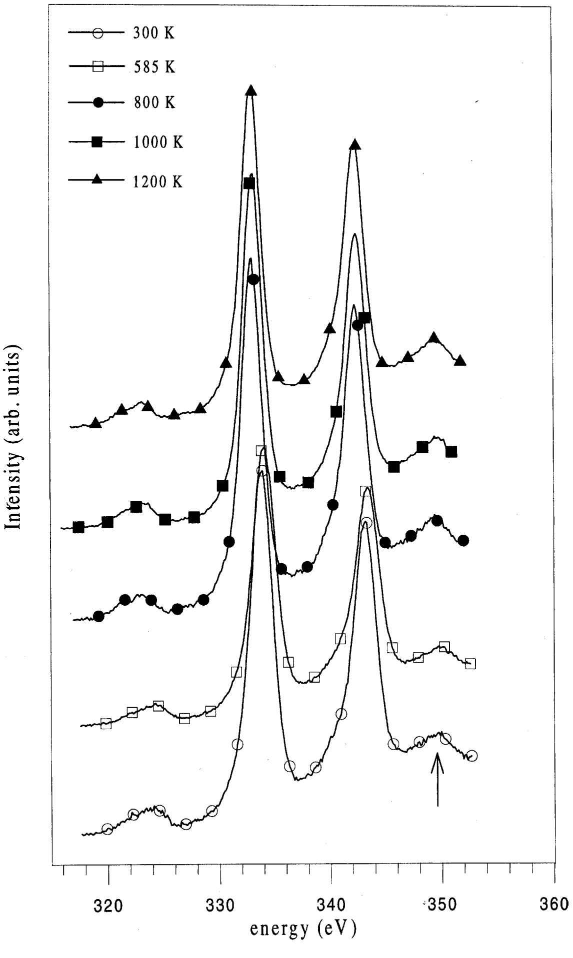

Fig. 10. Th(4f) photoelectron spectra of $Th(CO_3)_2$ and other decomposed intermediates. Satellite positions are marked with arrows.

beam induced dissociation of such carry over phases has been tried out on earlier instances [26,27]. In the present case, an attempt was successfully made to destroy these phases by heating these samples beyond decomposition regime.

Occurrence of C(1s) peak around 292 eV in all the samples indicated specimen charging arising from the insulating characteristics of the samples. Suitable charge correction procedure was therefore adopted for this purpose.

In the case of compound A there were three different signals for carbon at 284.73, 291.78 and at 296.31 eV. The first one can be attributed to the extraneous carbon on indium foil used to load the sample, as there is no charging on the indium peaks in the survey scan. The second one is due to extraneous carbon on the non-conducting thorium sample, which is taken as the reference point. The third one is due to the carbon from the thorium carbonate. The core level photoemission spectra of the Th compounds encountered in the study are shown in the Fig. 10. The binding energy values, peak areas and FWHMs are given in the Table 4. The $4f_{7/2}$ photoelectric peak in metallic thorium occurs at 333.0 eV. Compared to this, the stage A sample gave peak position at 333.97 eV with a satellite at 6.74 eV ahead of $4f_{5/2}$ peak [28]. In each formula molecular unit of $Th(CO_3)_2$ there are two carbonate oxyanion ligands. Though thorium atom remained tetravalent, the effective charge state of the compound is altered due to the presence of carbonate oxyanion in the primary coordination sphere. This results in a higher chemical shift. The shake up satellite signature is attributable to an electronic excitation from $Th_{5f/6p/7s}$–$O_{2s/2p}$ bonding band lying well below the Fermi level to an empty conduction band orbital [27]. The recorded satellite peak area amounted to 19.5% of the main $4f_{5/2}$ peak area.

The O(1s) photoelectric peak positions are shown in Fig. 11. The O(1s) peak corresponding to the initial compound (stage A, $Th(CO_3)_2$) yielded two prominent peaks. The peak located around 531.00 eV before applying charge correction, which is a combination of the photoelectrons from the charged surface due to the X-ray satellite (non-monochromated Al-$K_\alpha$ source) and from oxygen on bare Indium foil, which is not charged. Another peak appeared around 537 eV and this after charge correction was deconvoluted in to two peaks one at 531.11 eV with a FWHM of 2.67 eV and another one at 529.08 eV with a FWHM of 2.62 eV. The higher binding energy one can be attributed to the carbon–oxygen and the lower one to thorium–oxygen type of bonding in $Th(CO_3)_2$. The Th–O bonds preponderate over C–O bonds. The ratio of the peak areas of the two deconvoluted peaks is 1.7. The peak intensity ratios of oxygen to thorium turn out to be 2.9.

The compound obtained at 585 K (stage B) is generated from the $Th(CO_3)_2$ after desorption of one molecule of $CO_2$. The $4f_{7/2}$ peak in this compound occurred at 334.07 eV with a FWHM of 2.51. The slight increase

Table 4
Photoemission peak positions for thorium and oxygen electronic levels in $Th(CO_3)_2$ and its decomposition products

| Peak (eV) [area] FWHM | A | B | C | D | E |
|---|---|---|---|---|---|
| | 300 K | 585 K | 800 K | 1000 K | 1200 K |
| $Th(4f_{7/2})$ | 333.97<br>[71 098]<br>2.49 | 334.07<br>[88 106]<br>2.51 | 333.55<br>[52 464]<br>2.19 | 333.31<br>[136 441]<br>2.13 | 333.14<br>[126 556]<br>2.1 |
| $Th(4f_{5/2})$ | 343.3<br>[49 538]<br>2.44 | 343.31<br>[62 019]<br>2.54 | 342.85<br>[41 522]<br>2.35 | 342.59<br>[101 159]<br>2.27 | 342.5<br>[95 196]<br>2.22 |
| Satellite location | 350.04 | 349.81 | 349.96 | 349.81 | 349.62 |
| O(1s) C=O peak | 531.11<br>[16 573]<br>2.67 | 531.61<br>[15 068]<br>2.78 | 531.47<br>[2978]<br>2.72 | 531.45<br>[5486]<br>2.86 | – |
| O(1s) Th–O peak | 529.08<br>[9663]<br>2.62 | 529.5<br>[11 919]<br>2.72 | 529.46<br>[7601]<br>2.29 | 529.28<br>[22 457]<br>2.27 | 529.26<br>[24 751]<br>2.33 |
| Normalized O/M ratio | 2.9 | 2.4 | 1.6 | 1.6 | 1.6 |
| C on indium | 284.73 | | | | |
| C on Th sample | 291.78 | 292.04 | 292.04 | 293.41 | 292.56 |
| C as carbonate | 296.31 | 296.92 | | | |

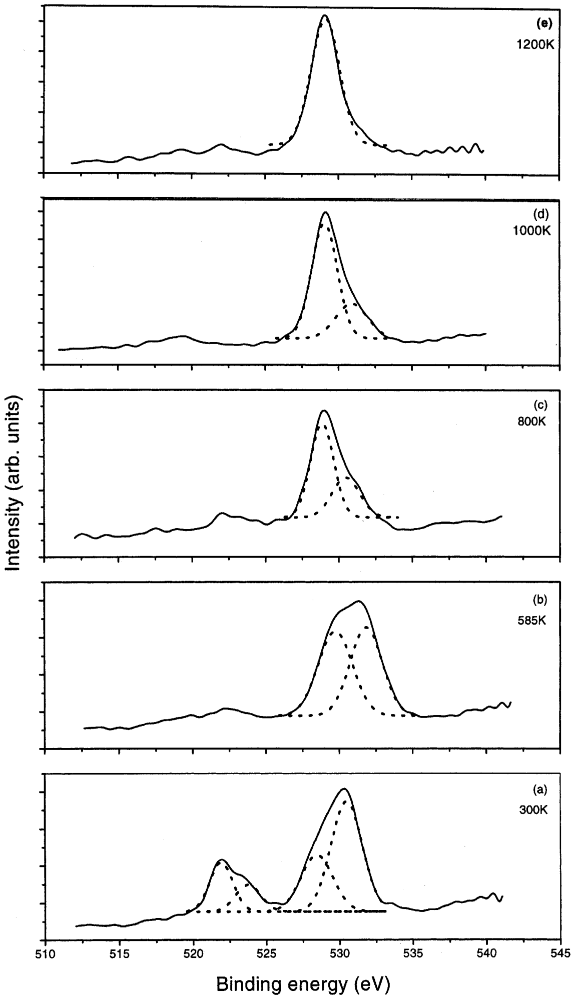

Fig. 11. O(1s) photoelectron spectra of $Th(CO_3)_2$ and other decomposed intermediates.

in binding energy can be attributed to the partial loss of $CO_3^{2-}$ ligand causing direct coordination of metal atom with oxygen. Hence, there is an increase in effective charge on the Th atom. Compared to stage A compound, there is an increase in peak area. The satellite was as usual observed at an energy 6.5 eV ahead of $4f_{5/2}$ photoelectric peak. This points to a reorganization in the valence band during stoichiometric transition of the compound from stage A → B.

In compound B, $ThOCO_3$, the scan for carbon revealed two peaks at 292.04, 296.92 eV corresponding to extraneous carbon on the sample and carbonate carbon in the sample respectively. The oxygen peak after charge correction appeared around 530 eV and it was deconvoluted into two peaks 531.61 eV with a FWHM of 2.78 eV and the other one at 529.50 eV with a FWHM of 2.72 eV, which corresponds to oxygen in C–O bond and Th–O bond respectively. This ratio of peak areas is found to be 1.3. This points to the reduction in C–O type of bonding arising from $CO_2$ loss. The oxygen to metal peak integrated intensity ratio dropped to 2.4.

The compound C, retrieved at 800 K gave a peak for carbon at 292.04 eV which is due to extraneous carbon on the sample. The carbonate carbon peak was not seen in this sample. The satellite occurred at 7.11 eV ahead of main $4f_{5/2}$ peak. This indicates renewed coordination around thorium atom implying onset of formation of a new compound i.e. thoria [29]. The oxygen peak around 530 eV was deconvoluted into two peaks, one at 531.47 eV with a FWHM of 2.72 and the other at 529.46 eV with a FWHM of 2.29. These peaks have an area ratio of 0.39 and the depletion of carbonate in the decomposition process shows that the residue contains two types of Th–O bonds.The oxygen signal arising from the parent carbonate precursor get diminished while the corresponding signal from the Th–O bonds gets enriched. The Th $4f_{7/2}$ peak was found at 333.55 eV with a FWHM of 2.19. Shift in the peak position indicates change in the neighbourhood of thorium atom while converting from carbonate to thoria. The oxygen to metal intensity ratio yielded a value of 1.6.

The residue collected after heating the specimen (beyond decomposition regime, stage D) to 1000 K yielded C 1s peak around 293.41 eV. This was used as the reference peak. Th($4f_{7/2}$) photoelectric peak after charge correction appeared at 333.31 eV with a FWHM of 2.13 and a satellite 7.22 eV ahead of $4f_{5/2}$ peak. The O(1s) peak occurring at 530 eV could be deconvoluted in to two peaks, one at 531.45 eV with a FWHM of 2.86 and another one at 529.28 eV with FWHM of 2.27. At this stage the oxygen environment belonging to the carry over carbonate precursor further declines. This is accompanied with concomitant increase in the oxygen environment belonging to thoria. The ratio of these two peaks was found to be 0.24. The 349.81 eV satellite is the result of an electronic excitation from the thorium–oxygen valence band to a conduction band minima. This satellite as well as the principal peak location at 333.3 eV are characteristic of thoria in which thorium atom has a octahedrally coordinated oxygen sphere. The oxygen to metal intensity ratio was found to be 1.6.

A thorium carbonate sample heated to 1200 K (stage E compound) was also analyzed by XPS. Spectral features similar to stage D compound were observed. For this compound, oxygen to metal intensity ratio was found to be 1.6 that is same as the value obtained for stage D compound. This points to the fact that near complete conversion of $Th(CO_3)_2 \rightarrow ThO_2$ have been achieved at stage D (1000 K) with elimination of carry over intermediates.

Though the TPD as seen from the EGA-MS and TGA data achieves completion at 800 K, the carry over phases and unstable intermediates are eliminated by extending the temperature program to 1000 K.

## 9. HRTEM studies

Fig. 12 shows a SAED from a 800 K annealed sample. It exhibits diffuse rings, indicating the nanocrystalline nature of the sample. These rings can be indexed to thoria phase.

Fig. 13(a) shows high resolution electron micrograph of raw $Th(CO_3)_2$ i.e., stage A sample. The particle contains nanocrystalline grains with typical dimensions ranging from 5–10 nm. The particles in this micrograph are 40–50 nm in size. The grains are randomly oriented and the particles are agglomerated. The SEM micrograph (Fig. 1) showed micron-sized polyhedral particles too. Hence the morphology of the precursor sample can be construed as micron-size aggregates with nanometer size grains.

Fig. 13(b) shows a micrograph of $Th(CO_3)_2$ specimen ramped to 800 K (stage C). Product crystallites having size in the range 5–10 nm show oriented assemblies. Development of facetting is observed in grains. In the selected area diffraction patterns rings belonging to product phase start appearing. There are indications of preferred orientations, suggesting that the predecessors $Th(CO_3)_2$ and $ThOCO_3$ phases are crystallographically related.

Fig. 14 shows the microstructure of sample acquired after terminating the heating schedule at 1000 K (stage D). The grain sizes are around 10 nm. The diffraction pattern indicates single phase nanocrystalline thoria. There is a predominant facetting of the grains. Further increase in temperature program to 1200 K (stage E) i.e., beyond decomposition regime results in grain growth to about 20 nm size.

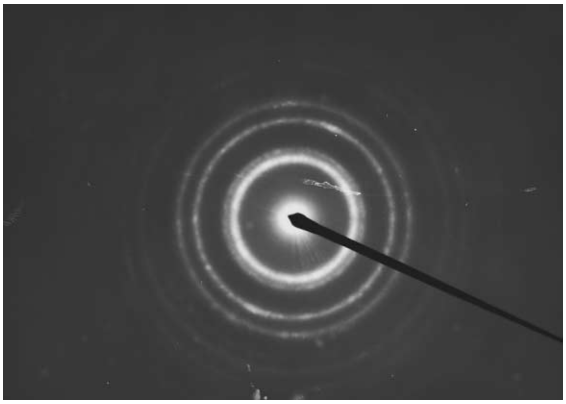

Fig. 12. SAED from $Th(CO_3)_2$ heated to 800 K.

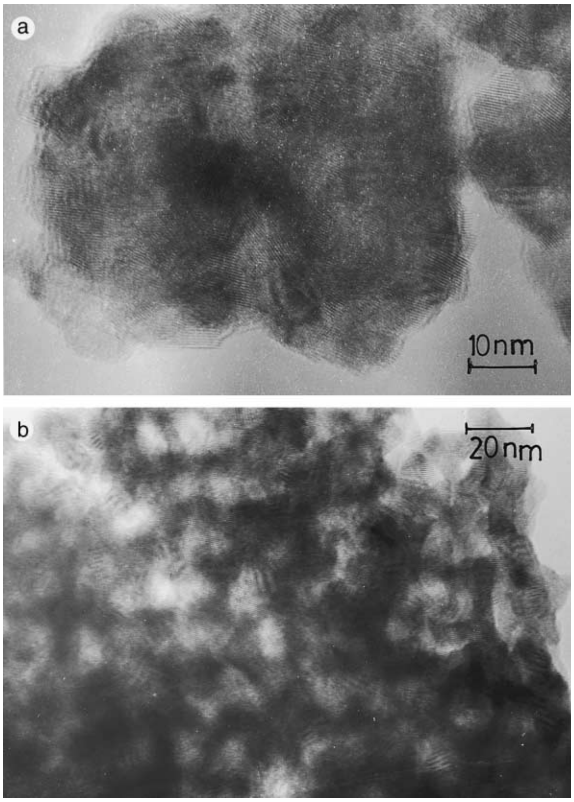

Fig. 13. HRTEM micrograph of (a) raw sample, (b) sample heated to 800 K.

## 10. Conclusion

Synthetic pathway for formation of nanocrystalline thoria from thermally decomposed thorium carbonate have been studied by EGA-MS and TGA. The rate governing kinetics for various conversion steps showed prevalence of nucleation and growth. Such reacting growth modes dominate owing to exceedingly large surface to volume ratio associated with the nanocrystalline particles. The non-isothermal kinetic methods are applied to determine Arrhenius parameters associated with each conversion step. Though TPD process indicated completion of transformation at 800 K, the XPS investigations revealed presence of carry over phases. This was inferred from the oxygen to metal intensity ratio measurements. However, advancing the temperature programme to 1000 K and beyond brought about a steady O/M ratio implying the fact that carry over phases do not persist beyond 1000 K. Infrared spectroscopic measurements show gradual disappearance of $CO_3^{2-}$ ligand. Also, discretization of vibrational levels were observed in nanocrystalline thoria. An increase in IR transmissivity over certain wave number regimes was observed in polycrystalline thoria. Raman spectroscopic

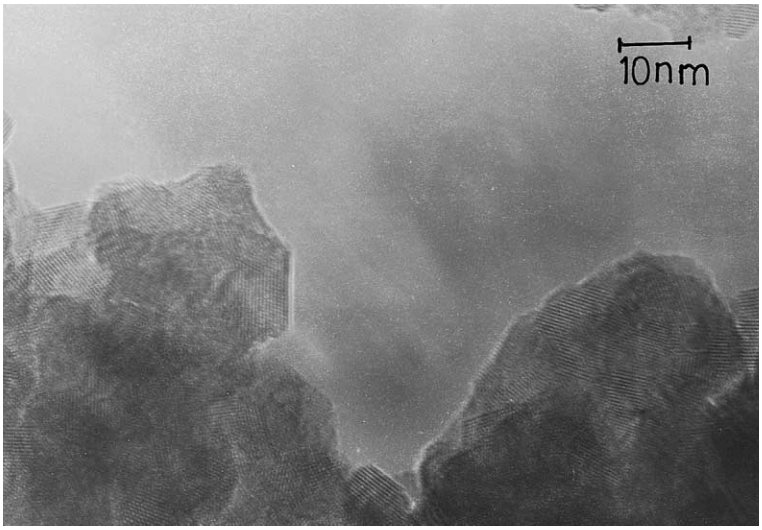

Fig. 14. HRTEM micrograph of sample heated to 1000 K.

measurements revealed optical phonon confinement as well as additional non-BZ phonon modes. This enhanced vibrational activity implies existence of increased atomistic transport processes in nanocrystalline thoria. This would augment dissolution rates of thoria pellets during reprocessing. The nanostructured morphology clearly revealed from the HRTEM study would augment dissolution rates of the thoria pellets during reprocessing.

## Acknowledgements

The authors are greatful to Mr V.S. Shastry for acquisition of X-ray diffractograms and Mrs M. Premila for recording FT-IR specra.

## References

[1] S. Dash, R. Krishnan, M. Kamruddin, A.K. Tyagi, B. Raj, J. Nucl. Mater. 295 (2001) 281.
[2] V. Chandramouli, S. Antonysamy, P.R. Vasudeva Rao, J. Nucl. Mater. 265 (1999) 255.
[3] H.P. Vyas, M.L. Dhawan, K. Balakrishan, D. Saha, K. Anantharaman, in: IAEA TCM Conf. on Advances in Heavy Water Reactors, Mumbai, India 1990.
[4] T.R. Mahalingam, Introduction to mass spectrometry, in: S.K. Aggarwal, H.C. Jain (Eds.), Indian Society for Mass Spectrometry, Mumbai, India, 1997, p. 13.
[5] S. Vijayalakhmi, R. Krishna Prabhu, T.R. Mahalingam, C.K. Mathews, At. Spectrosc. 13 (2) (1992) 61.
[6] M. Kamruddin, P.K. Ajikumar, S. Dash, B. Purniah, A.K. Tyagi, K. Krishan, Instrum. Sci. Technol. 23 (2) (1995) 123.
[7] M. Kamruddin, P.K. Ajikumar, S. Dash, R. Krishnan, A.K. Tyagi, K. Krishan, Thermochim. Acta 287 (1996) 13.
[8] S. Dash, M. Kamruddin, A.K. Tyagi, Bull. Mater. Sci. 20 (3) (1997) 359.
[9] M. Tischler, M.J. Koremblit, in: Temperature, its Measurement and Control in Science and Industry, vol. 5, part 1, AIP, New York, 1982, p. 383.
[10] M. Rajalakshmi, T. Sakuntala, A.K. Arora, J. Phys.: Condens. Matter 9 (1997) 9745.
[11] B.D. Cullity, In Elements of X-Ray Diffraction, Addision-Wesley, Reading, MA, 1956, p. 99.
[12] S. Dash, M. Kamruddin, P.K. Ajikumar, R. Krishnan, A.K. Tyagi, Ind. J. Chem. Technol. 5 (1998) 35.
[13] C.H. Bamford, C.F.H. Tipper (Eds.), Reactions in the Solid State, Comprehensive Chemical Kinetics, vol. 22, Elsevier, Amsterdam, 1980, p. 41.
[14] P.D. Garn, in: Thermoanalytical Methods of Investigation, Academic Press, New York, 1965, p. 247.
[15] R.O. Naquist, R.O. Kagel, in: The Handbook of Infrared and Raman Spectra of Inorganic Compounds and Organic Salts, Spectrum 58–63, Academic Press, San Diego, CA, 1997, p. 77.
[16] H. Gleiter, Acta Mater. 48 (2000) 1.
[17] A.K. Arora, M. Rajalakhmi, J. Appl. Phys. 88 (2000) 5653.
[18] M. Rajalakhmi, A.K. Arora, B.S. Bendre, S. Mahamuni, J. Appl. Phys. 87 (2000) 2445.
[19] H. Chessin, W.C. Hamilton, B. Post, Acta Crystallogr. 18 (1965) 689.
[20] I.P. Swainson, M.T. Dove, M.J. Harris, J. Phys.: Condens. Matter 7 (1995) 4395.
[21] C.L. Christ, J.R. Clark, H.T. Evans Jr., Science 121 (1955) 472.
[22] C. Greaves, S.K. Blower, Mat. Res. Bull. 23 (1988) 1001.
[23] T.C.W. Mac, Gong Du. Zhou, Crystallography in Modern Chemistry, Wiley, New York, 1992, 146.

[24] Alok Singh, S. Dash, M. Kamruddin, P.K. Ajikumar, A.K. Tyagi, V.S. Raghunathan, B. Raj, J. Am. Ceram. Soc. 85 (3) (2002).

[25] T. Swanson, Nat. Bur. Stand. (U.S.) Circular 539 (1) (1953) 53.

[26] S. Dash, M. Kamruddin, S. Bera, P.K. Ajikumar, A.K. Tyagi, S.V. Narsihman, B. Raj, J. Nucl. Mater. 264 (1999) 271.

[27] S. Dash, M. Kamruddin, S. Bera, P.K. Ajikumar, A.K. Tyagi, S.V. Narsihman, B. Raj, J. Nucl. Mater. 278 (2000) 173.

[28] J.C. Fuggle, A.F. Burr, L.M. Watson, D.J. Fabian, W. Long, J. Phys. F 4 (1974) 337.

[29] B.W. Veal, D.J. Lam, in: Gmelins Handbook of Inorganic Chemistry, A5, Verlag Chemie, Weinheim, 1973, p. 177.